Theor Chem Acc (2005) 113: 28–34
DOI 10.1007/s00214-004-0566-3

Theoretical
Chemistry Accounts

Regular Article

Structure and torsional flexibility of the linkage between guanine and fluorene residues in the deoxyguanosine–aminofluorene and deoxyguanosine–acetylaminofluorene carcinogenic adducts

Jan Florián, James Borden

Department Of Chemistry, Loyola University Chicago, 6525 N. Sheridan Rd., Chicago, IL 60626, USA

Received: 21 October 2003 / Accepted: 11 December 2003 / Published online: 13 December 2004

Abstract Potential energy surfaces for rotations around two central CN bonds in *N*-(deoxyguanosin-8-yl)-2-acetylaminofluorene (AAF–dG) and its deacetylated derivative (AF–dG) were studied using Amber 95 molecular mechanics. Both of these adducts are known to be strong mutagens and carcinogens. New Amber 95 force field parameters were derived for the linkage connecting guanine and fluorene moieties in AAF–dG and AF–dG. For this purpose, we determined ab initio MP2/cc-pVDZ//B3-LYP/6-31G* and polarized continuum model Hartree–Fock/6-31G* potential energy surfaces of smaller model systems that included the *N*-methylimidazole–acetylaniline and *N*-methylimidazole–aniline adducts. The molecular mechanics parameters were adjusted to minimize differences between the gas-phase ab initio and molecular mechanics surfaces of these model systems. The resulting parameters were transferred to AF–dG and AAF–dG. The barrier for the rotation of the fluorene residue in AF–dG was found to be less than 2 kcal/mol. Such a small barrier renders the fluorene moiety freely rotatable at room temperature. In contrast, the fluorene rotation in AAF–dG is hindered by a significantly larger barrier of 10 kcal/mol. This barrier corresponds to conformations in which the fluorene and acetyl groups lie in the same plane, and is largely due to steric repulsion. Similarly, the coplanar arrangement of guanine and the bridging amino or acetyl groups is disfavored by 5–10 kcal/mol, with AAF–dG again being the more rigid of the two molecules. Energy minima for a rotation around a bond between guanine and the bridging nitrogen are found at $\pm 80°$ in AAF–dG, and at 120° and −90° for AF–dG. Overall, the fluorene–dG linkages in AF–dG and AAF–dG adducts have significantly different equilibrium structures and torsional flexibilities. These differences may be contributing factors for the observed disparity in mutagenic effects of these adducts.

Keywords Carcinogen – Aminofluorene – Acetylaminofluorene – Guanine – Potential energy surface – Molecular mechanics

Electronic Supplementary Material Supplementary material is available in the online version of this article at http://dx.doi.org/10.1007/s00214-004-0566-3

Correspondence to: J. Florián
e-mail: jfloria@luc.edu

Introduction

Nucleobases are known to react with a variety of chemical agents. Products of these reactions are incorporated into DNA helices, creating modifications to the DNA structure [1]. When traversing these structural modifications, DNA polymerases may synthesize DNA with an incorrect base sequence containing point—or frameshift—mutations [2]. The accumulation of mutations leads to cancer [3].

N-Acetyl-2-aminofluorene (AAF) and its derivatives are among the most intensively studied of all chemical mutagens and carcinogens [4, 5, 6, 7, 8]. In vivo, AAF reacts with DNA, resulting in the *N*-(deoxyguanosin-8-yl)-2-acetylaminofluorene adduct (AAF–dG) and its deacetylated derivative, *N*-(deoxyguanosin-8-yl)-2-aminofluorene (AF–dG) (Fig. 1). AAF–dG typically blocks the synthesis of new DNA by DNA polymerases, or causes frameshift mutations [9]. Either of these usually results in cell death or impaired ability for the cell to divide. In contrast, AF–dG can be more readily bypassed by DNA polymerases [10]. However, this bypass often occurs at the expense of generating point mutations by inserting an incorrect nucleobase in place of a correct base. The difference in the biological activities of AF–dG and AAF–dG must reflect the inherent structural change, namely the replacement of the bridging NH group in AF–dG by the N–CH_3O group in AAF–dG. This change modifies the local chemical properties

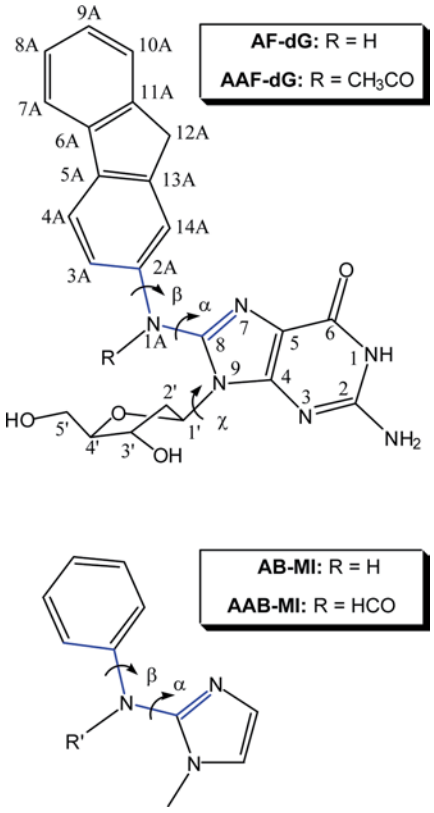

Fig. 1 Structure and numbering of the aminofluorene (*AF*) and acetylaminofluorene (*AAF*) adducts of deoxyguanosine (*dG*) (*top*), and the corresponding model compounds (*bottom*). The bonds drawn in *blue* indicate the torsional coordinates, for which we determined the potential energy surfaces

of the bridge that links guanosine and fluorene, for example, its hydrogen-bond donor/acceptor nature. In addition, the bridge modification is expected to affect the overall geometry of the adduct, and the thermal accessibility of various conformers. Because both the protein environment and the local properties of the bridge are likely to play important roles in the mutagenesis, a well-balanced theoretical approach is required to reproduce and understand the structure–function correlations discussed previously. As a first step, the structure and conformational flexibility involving torsions α and β in the bridge (Fig. 1) need to be scrutinized. Other torsions, such as the glycosidic bond torsion (χ) or ribose puckering, are undoubtedly also significant, but here we can rely on numerous theoretical papers that have previously addressed conformational properties of DNA (Ref. [11] and references therein) including the availability of sophisticated sets of molecular mechanics (MM) parameters. [12, 13].

Early MM studies focused on finding the optimal geometry of a dinucleotide or DNA that contained guanosine modified by fluorene derivatives [14, 15, 16, 17]. This was and still is a challenging task because of the presence of multiple minima on the conformational energy surface and large charges on the phosphate groups. Therefore, these studies were limited to the torsional subspace, while keeping bond angles and bond lengths frozen. More recent MM studies used unrestrained molecular dynamics (MD) and the force field of Weiner et al. [18] to study the equilibrium conformation of short DNA duplexes containing AAF–dG [19, 20]. The study of Fritsch and Westhof [20] also systematically evaluated the conformational space for the torsions α and χ, in AAF–dG, but did not address the magnitudes of the torsional barriers separating the minimized structures. The torsional barriers within the α–χ configuration space of AAF–dG were investigated by Besson and Mihalek [21], who used the modified neglect of differential overlap semiempirical quantum chemistry method. However, the activation energy calculated by Besson and Mihalek for the rotation around the glycosidic bond was about 100 kcal/mol. Such a large barrier is inconsistent with the experimental observation that in solution, syn and anti conformers of mononucleotides are in rapid equilibrium with each other [22, 23]. This disagreement underscores the need to consider solvation effects and to use ab initio level of theory to obtain correct torsional surfaces. Ab initio Hartree–Fock (HF) and density functional calculations of the torsional potential for the angle β in the standalone AAF molecule have been reported by Topper et al. [24].

At the present stage of computer technology, all-atom MD computer simulations of DNA/protein complexes in solution can be performed to expand our understanding of the structural and dynamic origins of AAF carcinogenicity. In order to obtain realistic results from these calculations it is important to use properly parameterized MM force fields. Major attention needs to be paid to the rotations around two CN bonds in the bridge (angles α and β in Fig. 1) because the magnitudes of the corresponding torsional angles greatly affect the overall geometry of the adducts. Currently, ab initio quantum chemical methods that include electron correlation and relaxation effects represent the method of choice to determine accurate potential energy surfaces (PESs) for internal rotations [25, 26]. Therefore, in this study we applied ab initio calculations to investigate the fully relaxed potential energy of AF–dG and AAF–dG as a function of torsional angles α and β. Because AF–dG and AAF–dG were too large to be treated at the correlated level of ab initio theory, the actual calculations were carried out for model systems in which the AF and AAF were replaced by aminobenzene (AB) and acetylaminobenzene (AAB), respectively, and guanosine was replaced by methylimidazole (MI) (Fig. 1, bottom). Because the aromaticity of the substituents of the central nitrogen (N1, Fig. 1) is retained, CN bonds in the bridge of AB–MI and AAB–MI molecules represent a good approximation for the corresponding bonds in AF–dG and AAF–dG, respectively. However, what is not retained in the reduced models of AF–dG and AAF–dG are the steric and electrostatic interactions between deoxyribose and AF or AAF. Fortunately, these interactions can be described with sufficient accuracy at the MM level using standard force field parameters, without

the necessity to use quantum chemical methods. Thus, after adjusting the parameters of the Amber 95 force field [12] for bridging CN bonds on our ab initio data, we proceeded to determine MM PESs for rotation around these bonds in the syn conformers of AF–dG and AAF–dG. These conformers have been observed in DNA duplexes in solution [19] and represent key structures in the base-displacement model of mutagenesis [27].

Computational methods

Adiabatic (i.e., fully-relaxed) PESs were calculated by varying torsions α and β (Fig. 1) in 20° increments in the (0°, 180°) and (0°, 360°) ranges, respectively, while relaxing all the remaining degrees of freedom so that the molecule studied could achieve its lowest energy. A total number of 360 and 180 individual geometry minimizations was performed for the AB–MI and AAB–MI molecules, respectively. The reason for the larger number of AB–MI minimizations was the presence of the double-minimum inversion potential of the hydrogen atom bonded to the bridging nitrogen. This potential could lock the geometry in a higher local-minimum rather than in the fully relaxed global minimum, for which we intended to determine the PES. In our calculations we systematically probed both minima of the inversion potential and in cases when the final geometries differed, we used the lower of the two total energies. In addition, the geometry of the methyl group bonded to the imidazole ring was constrained to possess the local C_{3v} symmetry to improve the convergence of the Berny geometry minimization algorithm. The use of this constraint resulted in less than 0.1 kcal/mol change in the total energy compared with the case of a fully minimized CH_3 group. The series of partial ab initio geometry minimizations (for fixed α and β) were carried out at the B3-LYP/6-31G* level in **Z**-matrix internal coordinates. The B3-LYP method belongs to the family of hybrid density functional theory (DFT) approaches, which combine nonlocal exchange and correlation functionals with the HF exchange term [28]. For each B3-LYP geometry, we calculated the total energy at the ab initio MP2(frozen-core)/cc-pVDZ level. The effect of aqueous solvation was studied by augmenting gas-phase MP2 energies with solvation free energies determined using the polarized continuum model (PCM) [29]. Pauling atomic radii scaled by the standard factor of 1.2 were used for PCM calculations. This approach has been shown to yield reasonable solvation free energies of neutral imidazole and aniline [30]. All ab initio calculations were carried out using Gaussian 98 [31].

The MD calculations were based on the Amber 95 MM force field [12]. The geometry relaxation for constrained angles α and β (also called adiabatic mapping) was generally accomplished by running gas-phase MD simulations that started at a temperature of 500 K. The molecule was subsequently cooled (by rescaling atomic velocities) in two steps to 100 and 0.1 K. These simulations were carried out with a time step of 0.2 fs and the total simulation time of 10 ps using program Q [32]. Nine independent geometry minimizations were carried out for each pair of (α, β) angles in the AF–dG and AAF–dG molecules. These minimizations, which differed in the length and the temperature of the initial step of the simulated annealing protocol, were carried out in order to explore the global and important local minima on the PES. The complete PESs for the syn conformers of AF–dG and AAF–dG lacking intramolecular hydrogen bonds between deoxyribose and guanine were calculated by using appropriate starting geometries (in the syn conformation). These geometries minimized in the low-temperature regime in order to keep their initial conformation. The low-temperature regime consisted of 5,000 0.2-fs steps at 20 K followed by 5,000 1.0-fs steps at 0.1 K. α and β torsions were fixed during MD simulations by applying two external torsional potentials with a potential energy barrier of 2,000 kcal/mol. These potential functions attained their single minimum for the predetermined angles α and β, and were removed in the last step of the calculations in which the final PES was determined. All pairwise nonbond interactions were taken into account in the MD simulations (i.e., no cutoff was applied).

MM parameters that were not generally available were determined as follows. Atomic charges were determined by fitting the molecular electrostatic potential in the point-charge approximation to the potential calculated at the ab initio HF/6-31G* level. The equilibrium bond lengths and angles were determined using the calculated B3-LYP geometry corresponding to the global energy minimum of AB–MI and AAB–MI molecules, and in some cases they were manually adjusted to achieve improved agreement between MM and MP2 energy surfaces. The force constants for angle and out-of-plane bending displacements were transferred from the general Amber 95 parameters for structurally similar angles. The force constants for bond stretching were determined from the B3LYP bonds lengths and the force constants for the structurally similar bonds that were already present in the Amber 95 force field. In this force constant adjustment, we utilized the fact that the magnitude of stretching force constants tends to decrease when the equilibrium bond length of the corresponding bond increases (Ref. [33] and references therein).

Results and discussion

The PES calculated for the rotation around the C8–N1A (α) and C2A–N1A (β) bonds, which interconnect the MI and phenyl residues in AAB–MI, is presented in Fig. 2. Because of the C_{2v} symmetry of the phenyl residue, ΔE as a function of β is invariant with respect to the 180° phenyl rotation. Thus, only the nontrivial section of the PES for β between 0° and 180° is shown. In addition, the energy surfaces presented throughout this paper are

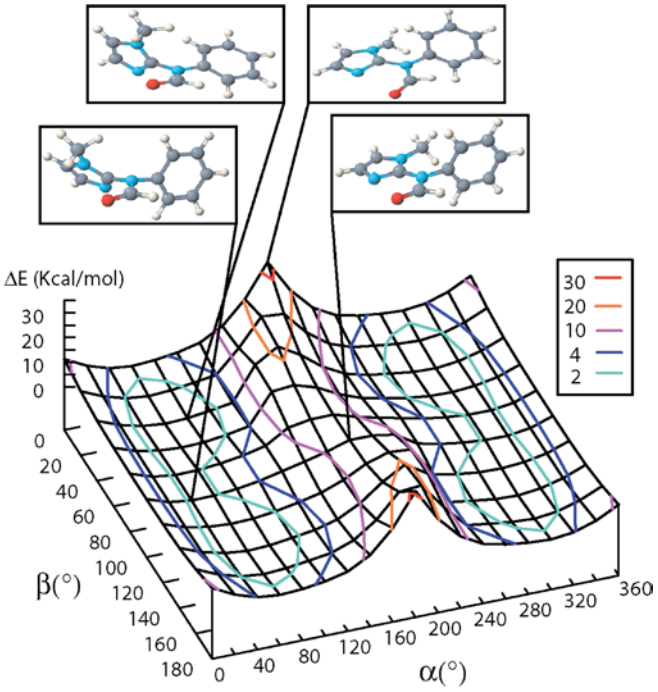

Fig. 2 MP2/cc-pVDZ//B3-LYP/6-31G* energy surface for the rotation around the bridging CN bonds in acetylaminobenzene (*AAB*)–methylimidazole (*MI*). Isoenergetic points are interconnected with *colored lines*. The geometries corresponding to selected stationary points are shown inside the *top frames*

limited to the subset of conformers, in which the amide oxygen is in a trans orientation with respect to the phenyl or fluorene ring. This selection is consistent with the experimental identification of the trans form of AAF–dG as a predominant conformer in solution and the solid state [34, 35, 36].

The characteristic features of the PES presented in Fig. 2 are further analyzed in Table 1. The surface shows two symmetry-equivalent global minima at (α, β) = (60°, 140°) (M1) and (300°, 40°) (M2) and two local minima at (60°, 40°) (M3) and (300°, 140°) (M4). The energy difference between the local and global minima is less than 0.1 kcal/mol at the MP2 level (Table 1). This difference increases to 0.8 kcal/mol at the DFT level. On the other hand, M3 and M4 become marginally more stable than M1 and M2 when the aqueous solvation effects are taken into account by the PCM model. The M1 conformer can be converted into M2 by 100° rotation of the phenyl ring, which is associated with a low (1.5 kcal/mol) barrier. The full 180° rotation of the phenyl residue is hindered by the barrier of 2.8 kcal/mol, corresponding to the coplanar arrangement of the phenyl and amide groups for $\beta = 0°$. This barrier is caused by the van der Waals repulsion between phenyl and amide group hydrogens. Despite the presence of such steric hindrance, the calculated barriers for phenyl rotation in AAB–MI are lower than the barrier observed for the rotation around the CN bond in aniline, which amounts to 3.5 kcal/mol [37]. This result indicates that the –HCO substituent, when attached to the aromatic amine nitrogen, decreases the bond order between the nitrogen and the aromatic ring (see also later).

Table 1. Comparison of ab initio and molecular mechanics (*MM*) energies for selected points on the potential energy surface of acetlyaminobenzene–methylimidazole. α and β (in degrees) correspond to torsional angles N7–C8–N1A–C2A and C8–N2A–C2A–C3A, respectively (Fig. 1)

Conformation		ΔE (kcal/mol)			
α	β	DFT	MP2	MP2 + PCM	MM
180	0	33.7	33.2	34.1	33.0
60	140	0.0[a]	0.0[b]	0.8	0.9
40	100	1.7	1.5	2.5	1.6
60	0	3.1	2.8	4.1	2.8
60	40	0.8	0.0	0.0[c]	0.0
180	100	14.1	13.1	11.8	8.9

[a]Total energy −665.268134 au
[b]Total energy −663.326425 au
[c]Point (80, 40). Total energy −663.341377118 au

The rotation around the N1A–imidazole bond (α) is more rigid. This rigidity is largely determined by steric effects. The highest point on the minimum-energy pathway for the α rotation corresponds to the (180°, 100°) conformer. The imidazole and amide groups are nearly coplanar in this conformer, while the phenyl and imidazole planes are oriented perpendicularly to each other with the methyl group stacked above the phenyl ring. The relative energy of this transition state is about 13 kcal/mol. This energy is only slightly affected by the change of the computational level from MP2 to DFT, or by the inclusion of solvation effects (Table 1).

The ab initio PES for AB–MI is presented in Fig. 3 and Table 2. The two symmetry-equivalent minima are located at (100°, 0°) and (260°, 0°). The barrier for the 180° rotation of the phenyl group was calculated as 3.2 and 4.3 kcal/mol at the MP2 and DFT levels, respectively. Both results agree reasonably well with the 3.5-kcal/mol barrier observed for aniline [37]. The calculated barriers are, even in the absence of substantial steric repulsion, higher than the corresponding barrier in AAB–MI. This finding is consistent with the longer C2A–N1A bond lengths in AAB–MI (1.437 Å) than in AB–MI (1.421 Å), as determined at the B3-LYP/6-31G* level. A larger bond order and consequently the torsional rigidity of the C2A–N1A bond in AB–MI needs to be reflected in the corresponding torsional MM parameter that should be different in AAF–dG and AF–dG (see later).

The relative MM energies of the selected points on the PES of AAB–MI and AB–MI are presented in Tables 1 and 2. These energies were calculated using the Amber 95 force field [12] augmented by the set of the parameters (atomic charges, equilibrium bond lengths and angles, harmonic force constants, torsional potentials) for the bridging part of the adducts determined in this work. The definition and values of these parameters are provided in supporting material. The key parameters determining the torsional flexibility of AF adducts are the potential energy barriers (V_0) in the twofold tor-

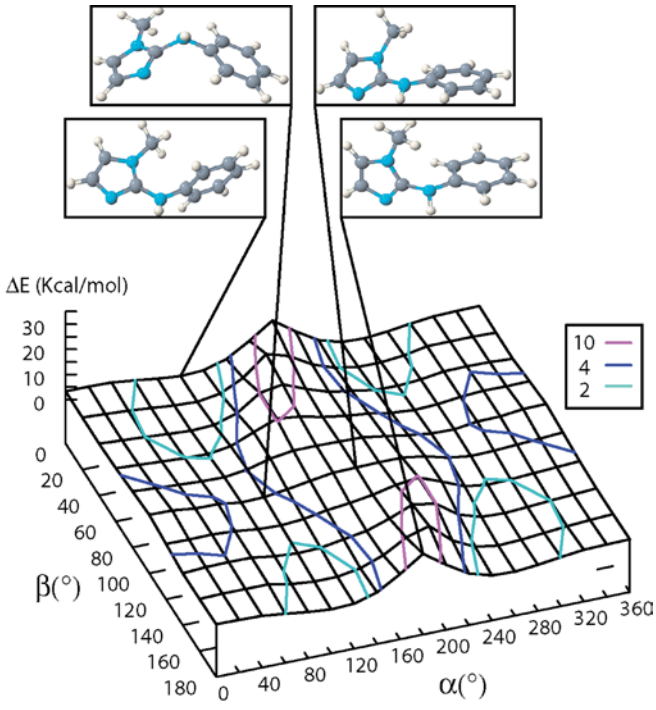

Fig. 3 MP2/cc-pVDZ//B3-LYP/6-31G* energy surface for the rotation around the bridging CN bonds in aminobenzene–MI. Isoenergetic points are interconnected with *colored lines*. The geometries corresponding to selected stationary points are shown inside the *top frames*

sional potentials of the torsions α and β. These potential functions attain their minima at 0° and 180°, and their maxima at 90° and 270°. The values used in this work were $V_0/2 = 3.8$ and 6.8 kcal/mol for the β torsion (i.e., the rotation of the phenyl group) in AAB–MI and AB–MI, respectively. A parameter $V_0/2 = 2.8$ kcal/mol was determined for the α torsional potential (i.e., the potential for the rotation of the MI) for both AAB–MI and AB–MI. These intrinsic bond torsions were combined with the electrostatic and van der Waals nonbond term to determine the overall potential energy profiles such as in Figs. 2 and 3. The resulting MM energies for AAB–MI (Table 1) lead to correct minima, although their relative stability coincides with the MP2 + PCM results rather than with the targeted MP2 values. The MM barriers separating these minima agree well with their MP2 counterparts. The MM potential for AB–MI also provides the correct geometry of the minimum structure and the correct barrier for phenyl rotation, but underestimates significantly the barrier for the rotation of the imidazole group. That is, whereas the MP2 barrier amounts to 7.9 kcal/mol, its MM equivalent is only 3.4 kcal/mol. Attempts to increase this barrier within the framework of the Amber 95 force field, which does not allow the values of atomic charges to be adjusted, led to the loss of the agreement in the region of the PES minima. Given that a proper description of the PES near the minima is fundamental for ground-state MD simulations, and that a barrier of 3.4 kcal/mol is still sufficiently high to prevent spontaneous transitions at room temperature and typical simulation times, we put up with the imperfection of our MM potential described. However, caution should be exercised if the conformers with α near 180° become significantly populated in simulations using force field parameters derived in the present work.

Table 2. Comparison of ab initio and MM energies fors elected points on the potential energy surface of aminobenzene–methylimidazole. α and β (in degrees) correspond to torsional angles N7–C8–N1A–C2A and C8–N2A–C2A–C3A, respectively (Fig. 1)

Conformation		ΔE (kcal/mol)			
α	β	DFT	MP2	MP2 + PCM	MM
180	0	10.7	14.6	15.0	11.4
0	100	4.4	5.8	5.3	6.2
100	0	0.0[a]	0.0[b]	0.0[c]	0.0
80	100	4.3	3.2	3.1	3.3
200	100	6.5	7.9	6.7	3.4

[a]Point (120, 0). Total energy −551.933214 au
[b]Total energy −550.274775 au
[c]Total energy −550.284347 au

AAF–dG and AF–dG nucleosides can adopt various conformational states that differ in angles α, β, and χ, puckering of the deoxyribose ring (P), and torsions around the C4′–C5′ (γ) and C5′–O5′ (δ) bonds (Fig. 1). With our goal being to compare rotational flexibilities in the dG–fluorene linkage between the two molecules, we decided to eliminate the multiple-minima problem by focusing only on a single *syn*-C2′endo–trans–trans conformational family in the χ–P–γ–δ space. This selection was accomplished without using any coordinate constraint by working instead in the low-temperature regime, which prevented the molecules from switching from one local minimum to another. The torsions of the starting configuration were selected as follows. The glycosidic bond torsion in the syn range (−90°, 90°), the C2′endo deoxyribose conformation (as in B-DNA), and the trans regions for the O4′–C4′–C5′–O5′ and C4′–C5′–O5′–H torsions. The trans regions for the C4′–C5′ and C5′–O5′ bonds were chosen in order to avoid the formation of the intramolecular hydrogen bonds between the O5′H and the guanine ring. This is because we intended the calculated PES to be relevant for nucleotides, which are devoid of the O5′–H group.

The resulting conformational energy map and the structures of the two lowest-energy conformers of *syn*-C2′endo–AAF–dG are presented in Fig. 4. Van der Waals interactions limit the energetically available conformers to those with α between 60° and 90° (g^+) and between −90 and −60° (g^-). Among the local minima, the g^+ conformer at (α, β) = (−80°, 60°) is 1 kcal/mol more stable than the g^- conformer at (80°, 110°). These g^+ and g^- conformers differ significantly in the orientation of the AF and acetyl groups with respect to the rest of the molecule (Fig. 4).

The g^+ and g^- conformations are also stable in *syn*-C2′endo–AF–dG, where the position of the minima

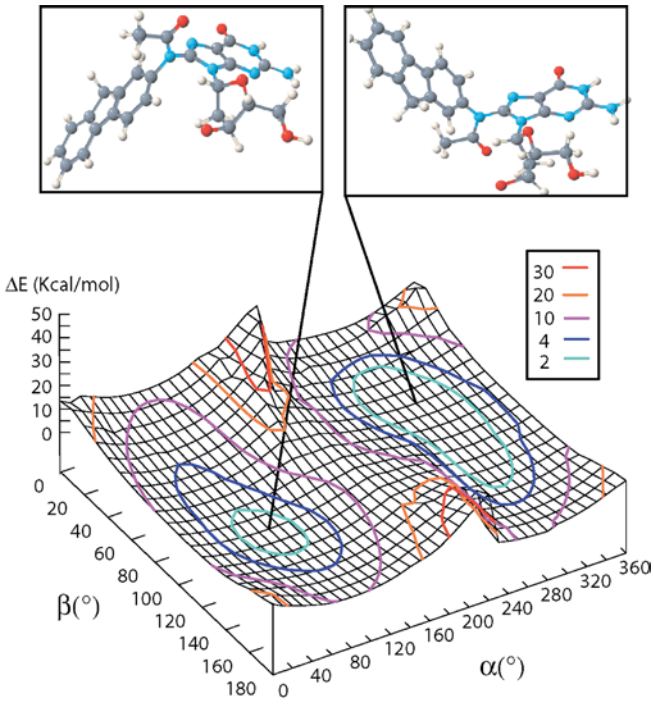

Fig. 4 Molecular mechanics (*MM*) energy surface for the rotation around the bridging CN bonds in *syn*-C2′endo–AAF–dG. Isoenergetic points are interconnected with *colored lines*. The geometries corresponding to local minima with $(\alpha, \beta) = (80°, 110°)$ and $(-80°, 60°)$ are outlined in the *top frames*

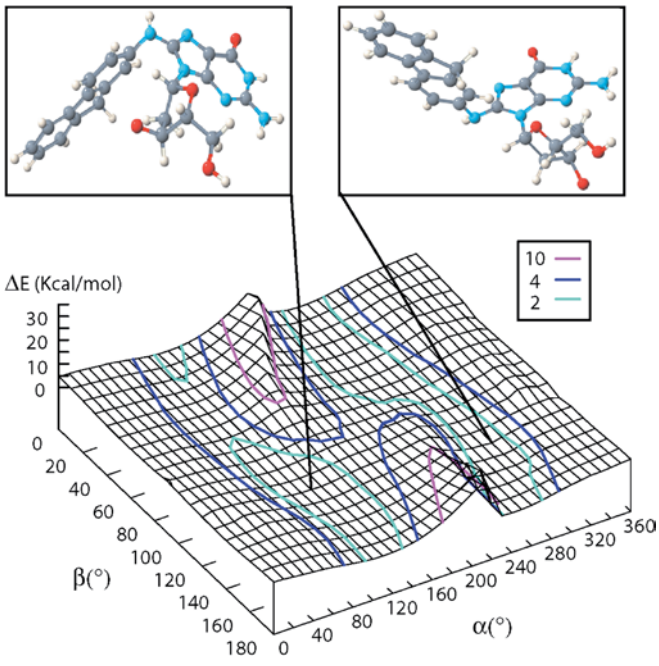

Fig. 5 MM energy surface for the rotation around the bridging CN bonds in *syn*-C2′endo–AF–dG. Isoenergetic points are interconnected with *colored lines*. The geometries corresponding to local minima with $(\alpha, \beta) = (120°, 120°)$ and $(-90°, 130°)$ are outlined in the *top frames*

shifts to $\alpha = 120°$ and $-90°$ (Fig. 5). The energy of the (120°, 120°) conformer is 0.7 kcal/mol lower than the energy of the (−90°, 130°) conformer. Although the rotation of the fluorene moiety has a higher intrinsic barrier in AB–MI than in AAB–MI (see earlier), this residue is practically free to rotate in *syn*-C2′endo–AF–dG. This is because the presence of the deoxyribosyl substituent increases the van der Waals repulsion near $\beta = 0°$ and 180°. The resulting combination of steric and intrinsic rotation barriers yields a flat potential for the fluorene rotation around the CN bond connecting it to the bridging nitrogen. In addition to the larger flexibility of the β torsion in AF–dG, this molecule also features a significantly smaller barrier for the transition between the g^+ and g^- conformations of the angle α than AAF–dG. However, because the MM parameters tend to underestimate this barrier by about 3 kcal/mol in AB–MI (see earlier), the actual barrier in AF–dG should be about 6 kcal/mol rather than 3.5 kcal/mol that can be inferred from the energy surface in Fig. 5. At any rate, even the corrected barrier of 6 kcal/mol is significantly smaller than the barrier of about 10 kcal/mol calculated for AAF–dG (Fig. 4).

In conclusion, internal rotations in AF–dG were found to be less hindered than in AAF–dG. Consequently, lower frequencies and larger amplitudes are expected for rotational motions of the linkage connecting guanine and fluorene parts in AF–dG at room temperature. This result, although obtained by MM simulations of free molecules, can be expected to be valid also in aqueous solution. This is because our ab initio calculations using the PCM model indicated negligible effects of the solvation on the torsional flexibility of the linkage bonds in the model systems. Differences in the equilibrium structures and rotational dynamics of AF–dG and AAF–dG, which stem from the intrinsic properties calculated in this work, may be retained to some extent in protein or DNA environments. In fact, the $(\alpha, \beta) = (80°, 110°)$ conformer corresponding to the energy minimum of AAF–dG (Fig. 4) has recently been observed in a crystal of a complex of T7 DNA polymerase with DNA which contained an AAF–dG residue [38]. This agreement indicates that the polymerase environment that binds the DNA duplex is flexible enough to accommodate the bulky AAF–dG moiety in its energetically preferred solution conformation.

Acknowledgements. This work was supported by the NSF REU grant no. CHE-0243825 to Loyola University Chicago. We thank to Tom Ellenberger and Shuchismita Dutta for providing us with their results prior to publication.

References

1. Friedberg EC, Walker GC, Siede W (1995) DNA repair and mutagenesis. American Society for Microbiology, Washington, DC
2. Echols H, Goodman MF (1991) Annu Rev Biochem 60:477
3. Weinberg RA (1996) Sci Am 275:62
4. Kriek E (1992) J Cancer Res Clin Oncol 118:481

5. Koffel-Schwartz N, Verdier JM, Bichara M, Freund AM, Daune MP, Fuchs RP (1984) J Mol Biol 177:33
6. Bichara M, Fuchs RP (1985) J Mol Biol 183:341
7. Tebbs RS, Romano LJ (1994) Biochemistry 33:8998
8. Wagner J, Etienne H, Janel-Bintz R, Fuchs RPP (2002) DNA Repair 1:159
9. Heflich RH, Neft RE (1994) Mutat Res Rev Genet Toxicol 318:73
10. Lindsley JE, Fuchs RPP (1994) Biochemistry 33:764
11. Sponer J, Florian J, Ng HL, Sponer JE, Spackova N (2000) Nucleic Acids Res 28:4893
12. Cornell WD, Cieplak P, Bayly CI, Gould IR, Merz KM Jr, Ferguson DM, Spellmeyer DC, Fox T, Caldwell JW, Kollman PA (1995) J Am Chem Soc 117:5179
13. Foloppe N, MacKerell AD Jr (2000) J Comput Chem 21:86
14. Hingerty B, Broyde S (1982) Biochemistry 21:3243
15. Broyde S, Hingerty B (1983) Biopolymers 22:2423
16. Lipkowitz KB, Chevalier T, Widdfield M, Beland FA (1982) Chem-Biol Interact 40:57
17. Norman D, Abuaf P, Hingerty BE, Live D, Grunberger D, Broyde S, Patel DJ (1989) Biochemistry 28:7462.
18. Weiner SJ, Kollman PA, Nguyen DT, Case DA (1986) J Comput Chem 7:230
19. O'Handley SF, Sanford DG, Xu R, Lester CC, Hingerty BE, Broyde S, Krugh TR (1993) Biochemistry 32:2481
20. Fritsch V, Westhof E (1991) J Comput Chem 12:147
21. Besson M, Mihalek CL (2001) Mutat Res Fundam Mol Mech Mutagenesis 473:211
22. Son TD, Guschlbauer W, Gueron M (1972) J Am Chem Soc 94:7903
23. Saenger W (1984) Principles of nucleic acid structure. Springer, Berlin Heidelberg New York
24. Topper RQ, Chung K, Boelke CM, Louie D, Kang JS, Hannan R, Kiang T, Chan LH (2003) Theor Chem Acc 109:233
25. Frey RF, Coffin J, Newton SQ, Ramek M, Cheng VKW, Momany FA, Schafer L (1992) J Am Chem Soc 114:5369
26. Yu CH, Norman MA, Schafer L, Ramek M, Peeters A, van Alsenoy C (2001) J Mol Struct 567:361
27. Grunberger D, Nelson JH, Cantor C, Weinstein IB (1970) Proc Natl Acad Sci USA 66:488
28. Becke AD (1993) J Chem Phys 98:5648
29. Miertus S, Scrocco E, Tomasi J (1981) J Chem Phys 55:117
30. Florián J, Warshel A (1997) J Phys Chem B 101:5583
31. Gaussian (1999) Gaussian 98, revision A.11.3. Gaussian, Pittsburgh, PA
32. Marelius J, Kolmodin K, Feierberg I, Åqvist J (1999) J Mol Graphics Model 16:213
33. Majoube M (1985) Biopolymers 24:1075
34. Evans FE, Miller DW (1983) J Am Chem Soc 105:4863
35. Evans FE, Miller DW, Levine RA (1984) J Am Chem Soc 106:396
36. Neidle S, Kuroda R, Broyde S, Hingerty BE, Levine RA, Miller DW, Evans FE (1984) Nucleic Acids Res 12:8219
37. Evans J (1960) Spectrochim Acta 16:428
38. Dutta S, Li Y, Johnson D, Dzantiev L, Richardson CC, Romano LJ, Ellenberger T (2004) Proc Nat Acad Sci USA 101:16186